Chinese Chemical Letters 34 (2023) 107893

Contents lists available at ScienceDirect

Chinese Chemical Letters

journal homepage: www.elsevier.com/locate/cclet

Design of copper oxide and oxygen codoped graphitic carbon nitride activator for efficient radical and nonradical activation of peroxymonosulfate

Lin Wei[a,1], Jialing Li[b,1], Chengyun Zhou[a], Biao Song[a], Fanzhi Qin[a], Wenjun Wang[c], Hanzhuo Luo[a], Deyu Qin[a], Cheng Huang[a], Chen Zhang[a,*], Yang Yang[d,*]

[a] College of Environmental Science and Engineering, Hunan University and Key Laboratory of Environmental Biology and Pollution Control, Ministry of Education (Hunan University), Changsha 410082, China
[b] School of Design, Hunan University, Changsha 410082, China
[c] School of Resources and Environment, Hunan University of Technology and Business, Changsha 410205, China
[d] Department of Chemical and Materials Engineering, University of Alberta, Edmonton, Alberta T6G 1H9, Canada

ARTICLE INFO

Article history:
Received 30 June 2022
Revised 21 September 2022
Accepted 7 October 2022
Available online 12 October 2022

Keywords:
Graphitic carbon nitride
Codoping
Peroxymonosulfate
Antibiotics
Advanced oxidation process

ABSTRACT

Rational regulation of stable graphitic carbon nitride (CN) for superior peroxymonosulfate (PMS) activation is important in the catalytic degradation of water contaminants. In this work, the copper oxide and oxygen co-doped graphitic carbon nitride (CuO/O-CN) was prepared *via* one-step synthesis and applied in activating PMS for oxytetracycline (OTC) degradation, displaying superior catalytic performance. Systematic characterization and theoretical calculations indicated that the synergistic effect between the oxygen site of CN and CuO can modulate the electronic structure of the whole composite further facilitating the formation of non-radical $^1O_2$ and various reactive radicals. Results of the influencing factor experiments revealed that CuO/O-CN has a strong resistance to the environmental impact. The degradation efficiency of OTC in the real water environment even exceeded that in the deionized water. After four successive runs of the optimal catalyst, the OTC removal rate was still as high as 91.3%. This work developed a high-efficiency PMS activator to remove refractory pollutants *via* both radical pathway and non-radical pathway, which showed a promising potential in the treatment of wastewaters.

Tetracycline (TC), as an important broad-spectrum antibiotic, has extensive applications in the prevention and treatment of human and animal diseases [1]. Due to the malabsorption of humans and animals, most TC and its metabolites inevitably enter the water environment. These highly hydrophilic TC residues may threaten aquatic ecosystems and human health by inducing antibiotic resistant bacteria or pathogens [2]. Oxytetracycline (OTC), one common TC, is often selected as a model compound to research the degradation of antibiotics from polluted aquatic systems. Adsorption, biological treatment, advanced oxidation processes, and other techniques have been carried out to remove OTC [3–5]. Among these techniques, sulfate radical-based advanced oxidation technology (SR-AOPs) has gathered tremendous interest owing to its high efficiency and wide adaptability in the field of water and wastewater treatment. However, when peroxymonosulfate (PMS, HSO_5^-) and peroxydisulfate (PDS, $S_2O_8^{2-}$) react directly with contaminants, the low reaction rate limits the development of SR-AOPs. Hydroxyl radical ($^{\bullet}OH$) and sulfate radical ($SO_4^{\bullet-}$) can be generated through activating persulfates (PMS or PDS) to quickly attack the target pollutants [6,7]. Therefore, activation is necessary for PMS and PDS when treating the contaminants, and it is critical to developing a highly efficient activator for SR-AOPs.

Graphitic carbon nitride (CN), a conjugated polymer rich in nitrogen atoms, has drawn great attention in the field of organic contaminants in degradation in water treatment on account of its excellent chemical stability, low cost, simple preparation, strong visible light response, and adjustable electronic structure [8,9]. But the low-degree of PMS activation and poor electron transfer ability can lead to undesirable catalytic effect of pristine CN [10]. To enhance the electron mobility of CN, the appropriate regulations of electronic structure, such as doping of metal or nonmetal heteroatoms, seem to be necessary. CN with rich nitrogen ligands can coordinate with various metals such as Mn, Fe, Co,

* Corresponding authors.
E-mail addresses: zhangchen@hnu.edu.cn (C. Zhang), yyang34@ualberta.ca (Y. Yang).
[1] These authors contributed equally to this article.

https://doi.org/10.1016/j.cclet.2022.107893
1001-8417/

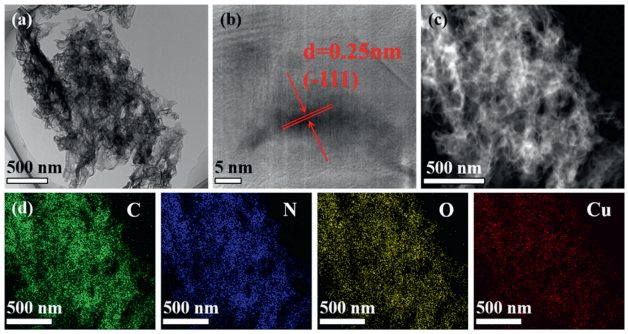

Fig. 1. (a) TEM image, (b) HRTEM image, (c) HADDF-STEM image and (d) EDS elemental mapping images of CuO/O–CN4.

and Cu to enhance the catalyst performance [11–13]. For instance, Xie and coworkers reported that cobalt doped graphitic carbon nitride (Co-CN) could enhance PMS activation for the removal of monochlorophenols [12]. However, the reusability of Co-CN is not satisfactory. After three reaction cycles, the rate constant is only about 23% of the initial value. In addition, oxygen doping can regulate the electronic structure of pristine CN. Oxygen doped graphitic carbon nitride (O-CN) could accelerate the degradation of bisphenol A *via* PMS activation [14]. But 10 mmol/L of PMS and 1 g/L O-CN was desired to completely degrade 0.05 mmol/L of bisphenol A, suggesting that the catalytic activity of O-CN can be further improved.

Metal doping or nonmetal doping alone can improve the catalytic performance of graphitic carbon nitride. However, the reusability of metal doped CN and the degradation efficiency of non-metal doped CN still need to be further improved. To obtain further improvement, taking the metal and nonmetal co-doped CN into consideration is a feasible choice. Some studies have been carried out to use metal and non-metal codoping to enhance the catalytic activity and stability of CN, such as Fe and O co-doped CN proposed by Chen *et al.* [15] and Mn and O co-doped CN proposed by Zhou *et al.* [16]. The oxidation–reduction ability of Mn, Fe, Co, Cu, *etc.* with variable valence transition is conducive to the PMS activation [17–19]. Copper oxide (CuO) has obtained extensive research in the field of catalysis because of its low toxicity and earth-richness [20]. For CuO-based materials, the incorporation of copper oxide may increase the specific surface area and active sites of the materials, so as to enhance the PMS activation. We speculated that O-CN can not only activate persulfate itself, but also promote the cycling of Cu(I) and Cu(II). Thus, it is expected that the co-dopants copper and oxygen into CN (CuO/O-CN) might efficiently activate PMS.

We herein synthesized a series of CuO/O-CN catalysts *via* one-step synthesis for activating PMS to degrade OTC. The mechanism on enhanced PMS activation of CN after metal and oxygen codoping was deeply explored by radical or non-radical quenching experiments, electron paramagnetic resonance (ESR), electrochemical analysis, and density functional theory (DFT) calculation. Furthermore, the possible degradation path of OTC was discussed. Influential factors of CuO/O-CN for OTC degradation including the catalyst and PMS dosages, pH, temperature, anions, humic acids (HA), and real water matrix were also investigated.

The morphologies and microstructures of CN and CuO/O-CN4 were investigated by SEM and TEM. As described in Fig. S1 (Supporting information), CN and CuO/O-CN4 obviously presented a layered stacking structure. Compared to CN, the morphology of CuO/O-CN4 showed a rougher surface. As shown in Figs. 1a and b, the CuO particles with the measured lattice fringe spacing of 0.25 nm (−111) were clearly detected in CuO/O-CN4 implying the successful modification of carbon nitride by copper oxide doping. The EDS results showed that C, N, O, and Cu in CuO/O-CN4 were uniformly dispersed (Figs. 1c and d), further implying the successful synthesis of target catalysts. The nitrogen adsorption-desorption experiments were carried out to investigate the BET specific surface areas of catalysts. As displayed in Fig. S3a (Supporting information), both CN and CuO/O-CNx samples possessed representative IV adsorption which represented the characteristics of the mesoporous structure. Additionally, the pore size distribution of all samples (Fig. S3b in Supporting information) was consistent with this result. Comparing CN with CuO/O-CN catalysts, the BET surface areas of them added as the amount of Cu increased, as exhibited in the inset of Fig. S3a. The BET surface area of CuO/O-CN4 was detected to be 90.35 m^2/g, which was 1.5 times higher than that of CN.

Fig. 2a displayed the XRD image of the CuO/O-CNx samples. The diffraction peak at 27.5° belonged to the interlayer stacking of graphite-like materials, and the weaker peak at 13.0° corresponded to the repeated packing of tri-*s*-heterocycle [8,21]. The two characteristic peaks can be attributed to the (002) and (100) crystal planes and are highly consistent with CN. With increasing the Cu content in CuO/O-CNx, it can be observed that the peak at 13.0° gradually disappeared, and the peak at 27.5° became weaker and wider compared with CN. Moreover, two new peaks of CuO/O-CN4 appeared at 35.6° and 38.8°, respectively, belonging to the ($\bar{1}11$) and (111) phases of CuO (JCPDS No. 65–2309) [22].

Raman spectra of samples that can verify the difference of frameworks on CN and CuO/O-CNx were depicted in Fig. 2b. For all samples, characteristic peaks corresponding to CN can be investigated. The peak at 707 cm^{-1} corresponded to in-plane bending, and another peak at 977 cm^{-1} belonged to symmetric nitrogen-breathing mode of heptazine [23]. Broad peaks ranging from 1100 cm^{-1} to 1700 cm^{-1} corresponded to the disorganized graphitic carbon-nitrogen vibrations [24]. From CN to CuO/O-CNx, the gradually weakened intensity of Raman signals was probably ascribed to the doped oxygen.

The chemical microstructures of the catalysts were further investigated by attenuated total reflectance FTIR spectra (Fig. 2c). For CN and CuO/O-CNx catalysts, the bending vibration peaks at ~810 cm^{-1} originated from the breathing mode of tri-*s*-triazine rings [25]. The peaks observed at ~1246, ~1327, ~1405, ~1469, ~1569, and ~1640 cm^{-1} correspond to the stretching vibration modes of connected units of C−NH−C, carbon-nitrogen heterocycles, and carbon-nitrogen stretching [26], respectively. Wide peaks in the range of 3100 min^{-1} to 3300 cm^{-1} belonged to the −NH and −OH vibration stretches [26,27]. Comparing CN with CuO/O-CNx catalysts we can observe that, peaks ranging from 1200 to 1700 cm^{-1} were gradually getting weaker as the amount of Cu increased. These changes may be due to the lattice defects caused by non-metal doping, indicating the successful doping of oxygen into the CN framework [28].

Characterization of CN and CuO/O-CN4 was conducted yet further by documenting the XPS spectra as depicted in Fig. 2d displayed the full survey spectra of CN and the CuO/O-CN4, indicating the signals for C, N, O, and Cu. The C 1s XPS of CN was depicted in Fig. 2e, in which the fitted three peaks at 287.8 eV, 284.8 eV, and 284.4 eV were attributed to sp^2-hybridized C, sp^3-coordinated C, and adventitious carbon [29], respectively. Compared with CN, one novel peak of CuO/O-CN4 at 286.1 eV was attributed to the C–O [30]. The generation of the signal peak of C–O bond may be evidence of O replacing N. The peak intensity belonging to C–C/C=C bonds enhanced and peaks ascribed to N–C=N and C–N (Fig. 2e) decreased, suggesting an increased content of C–C/C=C [31]. In addition, the binding energy of N–C=N bond in the CuO/O-CN4 catalyst shifted to lower energies, which may be attributed to the attractive relationship of the C species to the Cu atom [32]. The N 1s XPS revealed three main peaks at 400.8 eV, 399.7 eV, and 398.3 eV

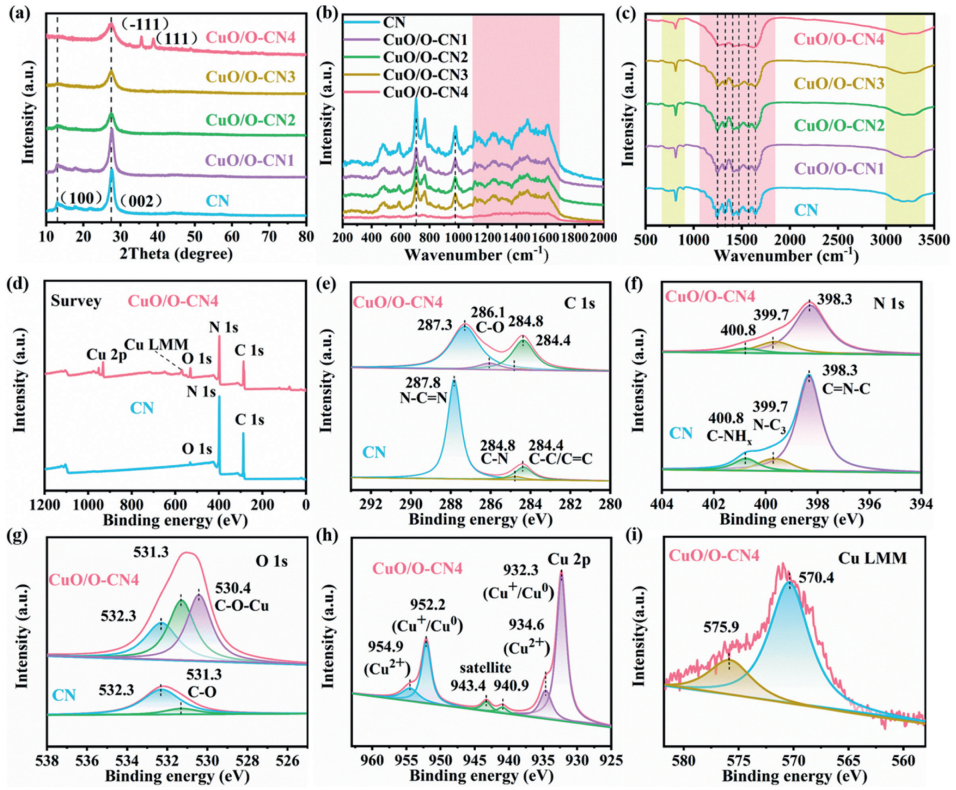

Fig. 2. (a) XRD patterns, (b) Raman spectra, (c) FTIR spectra of the samples, (d) XPS survey spectra of CN and CuO/O–CN4, and high-resolution XPS spectra of (e) C 1s, (f) N 1s, (g) O 1s, (h) Cu 2p and (i) Cu LMM in CN and CuO/O–CN4.

(Fig. 2f), corresponding to the amino functional groups (C–NH_x), tertiary nitrogen centers in N–C_3 units, and sp^2-hybridized nitrogen [33,34], respectively. The peak strength of C=N–C in the CuO/O-CN4 sample was significantly weakened, suggesting that the N vacancy was indeed generated in the material. In the O 1s spectrum (Fig. 2 g), the peaks of 532.3 eV and 531.3 eV were ascribed to adsorbed CO_2 or H_2O and surface-adsorbed oxygen (C–O) [27], respectively. The added peak at 530.4 eV in CuO/O-CN4 can be assigned to C–O–Cu species [27,35]. It should be noted that the increase of the peak corresponding to C–O indicated the successful modification of oxygen in the carbon framework. Compared with CN, the ratio of C/N for CuO/O-CN4 increased from 0.81 to 1.17, while the proportion of oxygen for CuO/O-CN4 obviously increased from 1.53% to 5.59% (Table S1 in Supporting information). It was thus concluded that oxygen atoms substituted for nitrogen atoms in CuO/O-CN4 and the oxygen atoms were easy to bond with the sp^2-hybridized carbon by replacing the two-coordinated nitrogen atoms based on the previous study [14]. What is more, in Fig. 2h, the Cu $2p_{1/2}$ high-resolution spectra were split into two peaks at 954.9 eV and 952.2 eV, which were ascribed to Cu^{2+} and Cu^{+}, respectively. Meanwhile, two peaks at 934.6 eV and 932.3 eV belonging to Cu $2p_{1/2}$ were also assigned to Cu^{2+} and Cu^{+} [36,37]. The peaks with binding energies of 940.9 eV and 943.4 eV were attributed to the satellite peaks of Cu^{2+} [38]. The spectra of Cu LMM (Fig. 2i) confirmed the presence of Cu^{+} at 570.4 eV and 575.9 eV [39]. The reducibility of hydroxyquinoline group may lead to the emergence of monovalent copper. XPS curve fittings showed the presence of Cu^{2+} and Cu^{+} on the CuO/O-CN4 surface.

As shown in Fig. S4 (Supporting information), the adsorption capacity of the catalysts for OTC improved with the increase of copper content. From Figs. 3a and b, when only PMS was added, about 65.5% of OTC was removed within 45 min with a rate constant of 0.02678 min^{-1}. The reaction rate was slightly added to

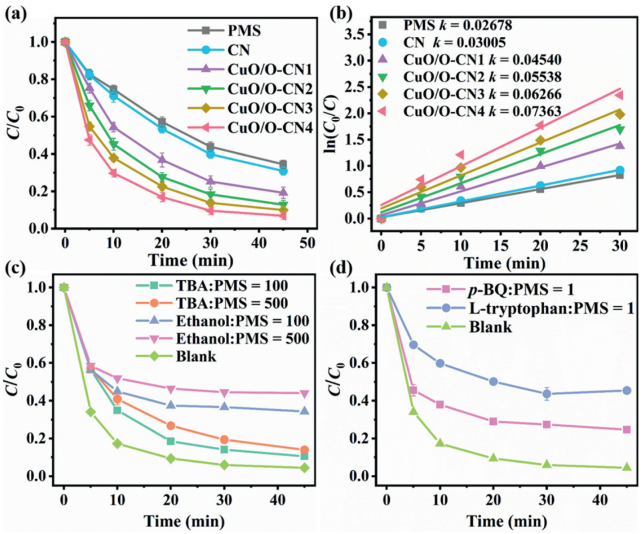

Fig. 3. (a) Degradation efficiency of OTC over different catalysts/PMS systems; (b) *Pseudo*-first-order kinetic fitting curves and the corresponding kinetic constants of (a). Inhibition of (c) ethanol, TBA, (d) *p*-BQ and L-tryptophan for OTC removal. Experimental conditions: catalyst = 300 mg/L, PMS = 0.1 g/L, initial pH 4.34, OTC = 30 mg/L.

0.03005 min^{-1} in CN/PMS system, and 69.1% of OTC was removed within 45 min. Compared with CN, the OTC degradation efficiency of copper oxide and oxygen co-doped samples was significantly improved. In copper containing samples, the higher the doping amount of copper acetylacetonate, the better the degradation efficiency. CuO/O-CN4 sample exhibited the highest activity for OTC degradation (93.1%) with a rate constant of 0.07363 min^{-1} which

was 2.45 times higher than that of CN. Moreover, as depicted in Fig. S5 (Supporting information), the catalytic performance of CuO/O-CN4 along with CN, CuO, and CN + CuO was evaluated. CuO/O-CN4 sample also showed the highest activity for OTC degradation. These results suggested that the introduction of CuO and O considerably increased the catalytic property of CN.

Fig. S6a (Supporting information) showed the effect of the catalyst concentrations on activating PMS to remove OTC. As the dosage of the catalyst increased from 0.1 g/L to 0.3 g/L, the k_{obs} value increased from 0.07817 min^{-1} to 0.08728 min^{-1} (Fig. S7a in Supporting information). The increase of catalyst dosage offered more active sites to form reactive species. The degradation efficiency of OTC did not increase with the increased catalyst dosage (0.4–0.5 g/L) addition, which may be explained by the complete activation of PMS at a lower catalyst dosage. Considering that the addition of 0.3 g/L catalyst achieved the desired degradation effect, 0.3 g/L of catalyst was used in the subsequent experiments.

The effect of PMS dosages on OTC removal was illustrated in Fig. S6b (Supporting information). With the PMS dosage increased from 0.02 g/L to 0.2 g/L, OTC removal efficiency sharply increased from 68.1% to 98.5%. The previous persulfate activation results based on free radicals indicated that the increase of PMS concentration would significantly promote the removal of organic pollutants, but excess PMS could consume reactive species and reduce the degradation efficiency [40–42]. Different results in this research suggested that the nonradical pathway may make a valuable contribution to the CuO/O-CN4/PMS system, which can be proved in the following part of mechanism discussion.

Real water commonly has a broad range of pH and the initial pH value is important in the advanced oxidation process of pollutants, so it is worthwhile to study the effect of different initial pH values in degrading OTC. In the CuO/O-CN4/PMS system, the impact of initial solution pH on the degradation of OTC was explored, and the results were displayed in Fig. S6c (Supporting information). The 95.6%, 93.7%, 95.2%, and 96.9% of OTC degradation were achieved at the pH of 4.3, 6, 8, and 10, respectively. CuO/O-CN4 showed better catalytic performance under strong alkali conditions. This may be explained by the promoted decomposition of PMS in alkaline solution, the production of more easily degraded intermediates in alkaline condition, or the enhanced adsorption of OTC on the surface of catalysts [43]. Under strong acidic conditions, the removal efficiency of OTC was significantly reduced, possibly because PMS was stable, so it is difficult to generate radicals at low pH values [44]. The pH-dependent CuO/O-CN4 surface charges can also explain this phenomenon. Zeta potential values of CuO/O-CN4 were positive below pH 5.39 (Fig. S8 in Supporting information). Under strong acidic conditions, the electrostatic repulsion would inhibit the affinity of both OTC ($pK_{a1} = 3.57$) and PMS ($pK_a = 9.40$) toward the CuO/O-CN4 surface [45], resulting in passivated degradation of OTC. In general, CuO/O-CN4/PMS systems exhibited apparently effective performance over a broad pH range of 4.3–10 and the best degradability under neutral and alkaline conditions. Even under strong acidic conditions, 73.2% OTC could still be degraded within 45 min.

The effect of reaction temperature on OTC removal by the CuO/O-CN4/PMS system over the temperature range of 20–60 °C was illustrated in Fig. S6d (Supporting information). High temperature apparently accelerated the degradation of OTC. The k_{obs} values increased with the increase of temperature, ranging from 0.08553 min^{-1} to 0.15324 min^{-1} (Fig. S7d in Supporting information). This may be due to that the high temperature improved the collision frequency between PMS molecules and catalysts so that more PMS can be adsorbed on the catalyst surface promoting reaction rates [46].

Natural organic matter (NOM) and inorganic ions are ubiquitous in natural waters and may exert an obvious influence on the adsorption and oxidation of organic pollutants [47]. The effects of Cl^-, HCO_3^{2-}, CO_3^{2-}, NO_3^-, and HA on the degradation of OTC were observed. As displayed in Fig. S6e (Supporting information), the presence of NaCl slightly inhibited the degradation of OTC with k_{obs} value of 0.08711 min^{-1}. The low concentration of Cl^- with a high-rate constant with $SO_4^{\bullet-}$ to generate less reactive radicals may be used to explain the slight reduction of OTC decomposition (Eqs. 1-3) [48].

$$Cl^- + SO_4^{\bullet-} \rightarrow {}^{\bullet}Cl + SO_4^{2-} \quad (1)$$

$${}^{\bullet}Cl + Cl^- \rightarrow {}^{\bullet}Cl_2^- \quad (2)$$

$$Cl^- + {}^{\bullet}OH \rightarrow {}^{\bullet}ClOH^- \quad (3)$$

HCO_3^- and CO_3^{2-} can react with $^{\bullet}OH$ and $SO_4^{\bullet-}$ (Rate constants: $k(HCO_3^-/{}^{\bullet}OH) = 8.6 \times 10^6$ L mol^{-1} s^{-1}, $k(CO_3^{2-}/{}^{\bullet}OH) = 3.5 \times 10^8$ L mol^{-1} s^{-1}, $k(HCO_3^-/SO_4^{\bullet-}) = 8.5 \times 10^6$ L mol^{-1} s^{-1}, and $k(CO_3^{2-}/SO_4^{\bullet-}) = 6.1 \times 10^6$ L mol^{-1} s^{-1}) to convert into carbonate radicals, thus inhibiting the degradation of pollutants [49,50]. Nevertheless, unlike the results illustrated in former reports, the results displayed in Fig. S6e indicated that bicarbonate and carbonate made a positive effect on the degradation process of OTC [51,52]. Indeed, the effect of 5 mmol/L of HCO_3^- and CO_3^{2-} on the OTC degradation resulted from the change of pH as described above, not carbonate ions. Additionally, the weaker ability of carbonate to promote the degradation than bicarbonate may be due to the higher rate constants of reaction with $^{\bullet}OH$ and $SO_4^{\bullet-}$.

Compared with the oxidation system without inorganic anions, the addition of 5 mmol/L of NO_3^- (Fig. S6e) had no significant effect on OTC degradation. The slight inhibition of OTC removal by the addition of NO_3^- was due to the reaction of nitrate ions with the produced $^{\bullet}OH$ and $SO_4^{\bullet-}$ to form $NO_2^{\bullet}$(1.03 V) and $NO_3^{\bullet}$(2.30 V) with lower potential (Eqs. 4-6) [42].

$$NO_3^- + {}^{\bullet}OH \rightarrow NO_3^{\bullet} + OH^- \quad (4)$$

$$NO_3^- + SO_4^{\bullet-} \rightarrow NO_3^{\bullet} + SO_4^{2-} \quad (5)$$

$$NO_3^{\bullet} + {}^{\bullet}OH + e_{aq}^- \rightarrow NO_2^{\bullet} + 2OH^- \quad (6)$$

HA can play two different roles in water. On the one hand, semiquinone free radicals, generated by quinonoid and phenolic groups in HA, can perform as an assistant to achieve a higher rate of PMS decomposition into $^{\bullet}OH$ and $SO_4^{\bullet-}$ [53]. On the other hand, HA generally performs as a free radical scavenger in water, consuming most of $^{\bullet}OH$ and $SO_4^{\bullet-}$. HA can be adsorbed on the catalyst surface and block active sites through carbonyl and hydroxyl moieties. When the HA concentration increased from 1 mg/L to 10 mg/L, the k_{obs} value of the CuO/O-CN4 increased which suggested that the detrimental influence of HA was overwhelmed by its positive influence (Fig. S7f in Supporting information). Compared with the blank experiment results, the k_{obs} value of the CuO/O-CN4 decreased to 0.08353 min^{-1} when the HA concentration was 20 mg/L. At this time, HA played a dominant negative role. In general, CuO/O-CN4 was an efficient catalyst with a strong ability to resist environmental impact.

The potential of the CuO/O-CN4/PMS process for practical application was examined in five types of real water such as deionized water (DW), medical sewage (MS), tap water (TW), Peach lake water (PW), and Xiangjiang river water (XW). The water quality index concentrations of this medical sewage were described in Table S2 (Supporting information). Interestingly, all the degradation efficiency of OTC in the real water was higher than that of DW with an increase respectively from 93.1% to 94.7%, 100%, 98.4%, and 98.3% (Fig. S9 in Supporting information). This could be ascribed

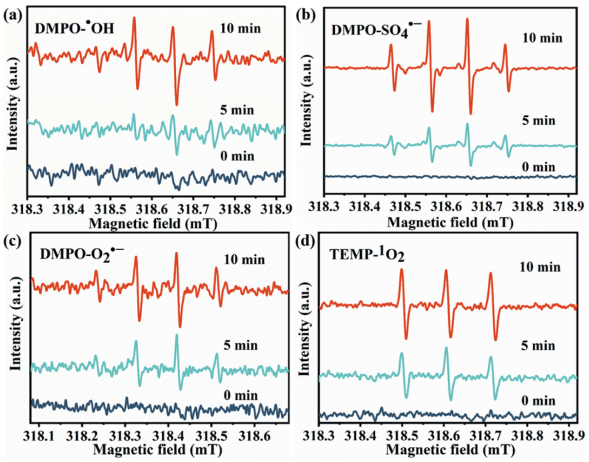

Fig. 4. ESR spectra of the (a) DMPO-•OH adduct, (b) DMPO-$SO_4^{\bullet-}$ adduct, (c) DMPO-$O_2^{\bullet-}$ adduct, and (d) TEMP-$^1O_2$ adduct. Experimental conditions: Catalyst = 300 mg/L, PMS = 0.1 g/L.

to the positive effect of the coexisting substrates (*e.g.*, HCO_3^- and NOM) in water. It is thus indicated that the process has the potential for full-scale application.

Different trapping experiments were conducted to determine the reactive species originate from the reaction system. Ethanol (k(•OH) = (1.2–2.8) × 10^9 L mol^{-1} s^{-1}, $k(SO_4^{\bullet-})$ = (1.6–7.8) × 10^7 L mol^{-1} s^{-1}) was used for quenching •OH and $SO_4^{\bullet-}$, and *tert*–butyl alcohol (TBA) (k(•OH) = (3.8–7.6) × 10^8 L mol^{-1} s^{-1}, $k(SO_4^{\bullet-})$ = (4–9.1) × 10^5 L mol^{-1} s^{-1}) was used for quenching •OH [54]. As shown in Fig. 3c, the effect of high-ratio radical scavengers ($M_{scavenger}/M_{PMS}$ = 100 or 500) on the CuO/O-CN4/PMS system was performed. The inhibitory effect of ethanol on OTC degradation was greater than that of TBA. The OTC degradation was 86% within 45 min with 50 g/L TBA addition and was just 56% with 50 g/L ethanol addition. These results indicated that the existence of both •OH and $SO_4^{\bullet-}$ as the main reactive species can be the cause of OTC removal. Ethanol showed a much higher inhibitory effect on OTC degradation than TBA revealing that $SO_4^{\bullet-}$ contributed much more than •OH in the reaction system.

In addition, as depicted in Fig. 3d, *p*-benzoquinone (*p*-BQ) and L-tryptophan were employed as scavengers for $O_2^{\bullet-}$ and $^1O_2$. In the presence of 0.1 g/L *p*-BQ, OTC degradation by CuO/O-CN4/PMS was inhibited with 75% in 45 min, indicating that $O_2^{\bullet-}$ was produced in the reaction system. When adding 0.1 g/L L-tryptophan into the CuO/O-CN4/PMS system, the same inhibition results can be observed. The degradation of OTC was inhibited with only 55% in 45 min, after adding L-tryptophan to the reaction system. To further confirmed the $^1O_2$ generation, 0.1–0.5 g/L furfural alcohol (FFA) was used as a chemical probe (Fig. S10 in Supporting information). The addition of FFA led to significantly suppressed degradation of OTC. These results indicated that both $O_2^{\bullet-}$ and $^1O_2$ were generated by the CuO/O-CN4/PMS system and $^1O_2$ played a leading role in the reaction system.

The above discussion showed that •OH, $SO_4^{\bullet-}$, $O_2^{\bullet-}$, and $^1O_2$ may work together for the efficient degradation of OTC in CuO/O-CN4/PMS system. To further study the reactive oxygen species involved in the reaction system, ESR analysis was applied using DMPO and TEMP as the spin-trapping reagents. As depicted in Figs. 4a and b, the DMPO-•OH signal and DMPO-$SO_4^{\bullet-}$ signal were clear and confirmed the co-existence of •OH and $SO_4^{\bullet-}$ [55]. In addition, the DMPO-•OH peak intensity and DMPO-$SO_4^{\bullet-}$ peak intensity increased with time (from 0 min to 10 min), indicating the continuous production of •OH and $SO_4^{\bullet-}$ in the CuO/O-CN4/PMS system. Obviously, the DMPO-$SO_4^{\bullet-}$ peak intensity was stronger than DMPO-•OH peak intensity, indicating that $SO_4^{\bullet-}$ was the main reactive radical which was in accordance with radical scavenging studies [14]. Besides, DMPO-$O_2^{\bullet-}$ characteristic signals (with 1:2:2:1 intensity ratio) and TEMP-$^1O_2$ characteristic signals (with 1:1:1 intensity ratio) can be seen in Figs. 4c and d, indicating the generation of $O_2^{\bullet-}$ and $^1O_2$ in the CuO/O-CN4/PMS system. Particularly, the peak intensity of $^1O_2$ increased with time was higher than that of DMPO-$O_2^{\bullet-}$ [14]. The findings confirmed that $^1O_2$ was also the dominating reactive radicals in the CuO/O-CN4/PMS process, as well as in agreement with the consequences of radical trapping experiments. Taken overall, both $SO_4^{\bullet-}$ and $^1O_2$ contributed to the degradation of OTC.

Nonradical pathways possibly derived from electron transfer between $^1O_2$ and PMS and pollutants [56] in the CuO/O-CN4/PMS system promoted OTC degradation. To further confirm the nonradical oxidation pathways in this system, linear sweep voltammetry (LSV) and electrochemical impedance spectroscopy (EIS) of CN and CuO/O-CN4 were conducted. LSV plot (Fig. S11a in Supporting information) obtained in CuO/O-CN4 was investigated by increasing the current of 0.1 g/L PMS solution, indicating the interaction and electron rearrangement between PMS and CN-based catalysts. PMS and OTC addition obviously resulted in increased current, proving the rapid electron transfer on the ternary system of CuO/O-CN4/PMS/OTC and providing strong evidence for the existence of nonradical pathways in the CuO/O-CN4/PMS/OTC system. Additionally, the smaller arc radius of CuO/O-CN4 on the EIS demonstrated that the CuO/O-CN4 had lower impedance and stronger electron transfer ability than CN, suggesting that copper oxide and oxygen codoping could promote the catalytic activity (Fig. S11b in Supporting information).

Copper oxides could be inserted into the "hole" between triazine units rather than bound by O-CN [57]. According to the following equations (Eqs. 7-9), $SO_4^{\bullet-}$ and •OH can be produced by CuO activated PMS [57]:

$$Cu(II) + HSO_5^- \rightarrow Cu(I) + SO_5^{\bullet-} + H^+ \quad (7)$$

$$Cu(I) + HSO_5^- \rightarrow Cu(II) + SO_4^{\bullet-} + OH^- \quad (8)$$

$$Cu(I) + HSO_5^- \rightarrow Cu(II) + SO_4^{2-} + {}^\bullet OH \quad (9)$$

Previous studies have established that the introduction of O atoms can increase the positive charge of nearby C atoms, so as to form C atoms with low electron density [14], which is in agreement with the calculation results on the basis of DFT. As illustrated in Fig. S12 (Supporting information), the positive charge of the C atom nearby oxygen dopants obviously increased from 0.735 to 0.822, suggesting that the C atom had poor electrons. In addition, the HOMO of O-CN (−0.12051) was higher than that of CN (−0.23348) (Fig. S13 in Supporting information), suggesting that the electron donating ability of O-CN increased. The energy gap (the difference between HOMO and LUMO) was 0.07645 for O-CN, which is lower than that for CN (0.18719), suggesting greater capacity of participating in chemical reactions. In this case, peroxy bonds (−O−O−) in PMS molecules can attack carbon atoms with low charge density through nucleophilic attack to produce $SO_5^{\bullet-}$, then the generated $SO_5^{\bullet-}$ would react with H_2O to product $^1O_2$ (Eq. 10). Moreover, the O atoms introduced into the framework of CN are rich in electrons. The identity of O-CN as an electron donor can promote the electron transferring from O atoms to PMS, thereby accelerating the conversion of Cu(II) to Cu(I) *via* PMS activation. In addition, Cu(II) can react with H_2O_2 produced by hydrolysis of persulfate to form $HO_2^{\bullet}$. Then, $HO_2^{\bullet}/O_2^{\bullet-}$ can form $^1O_2$ and regenerate H_2O_2 through recombination and self-decomposition (Eqs. 11-15) [58]. With the above analyses, a possible mechanism was proposed for the OTC removal in the CuO/O-CN4/PMS system

(Fig. S14 in Supporting information).

$$2SO_5^{\bullet -} + H_2O \rightarrow 1.5\,{}^1O_2 + 2SO_4^{2-} + 2H^+ \quad (10)$$

$$HSO_5^- + H_2O \rightarrow H_2O_2 + SO_4^{2-} + H^+ \quad (11)$$

$$Cu(II) + H_2O_2 \rightarrow Cu(I) + HO_2^{\bullet} + H^+ \quad (12)$$

$$HO_2^{\bullet} \rightarrow {}^{\bullet}O_2^- + H^+ \quad (13)$$

$${}^{\bullet}O_2^- + HO_2^{\bullet} \rightarrow {}^1O_2 \quad (14)$$

$$2{}^{\bullet}O_2^- + 2H^+ \rightarrow H_2O_2 + {}^1O_2 \quad (15)$$

As illustrated in Fig. S11c (Supporting information), four successive runs of CuO/O-CN4 catalyst were investigated to evaluate the reusability. OTC removal rates of 95.2%, 94.2%, 91.8%, and 91.3% were achieved within 45 min. This indicated that the copper-oxygen-codoped CN materials were not one-off materials. These copper-oxygen-codoped CN materials possessed stable catalytic activity for PMS. Furthermore, after four reaction cycles, used CuO/O-CN4 catalysts were characterized by XPS and FTIR (Fig. S15 in Supporting information). The peak corresponding to copper on the XPS spectra of the used sample became smaller, which may be due to a little copper leakage (Table S3 in Supporting information), resulting in a slight inhibition of the degradation. The FTIR spectra of the fresh sample and the used sample remain almost unchanged, which proved the stability of the material structure.

Considering the potential risks of degradation intermediates, it is significant to bring insights into the degradation pathways of OTC and its degradation products in the water environment. The transformation products of OTC in the CuO/O-CN4/PMS system were tested by HPLC-MS. Possible intermediates and their conversion processes were shown in Scheme S1 and Table S4 (Supporting information). The results suggested that two feasible decomposition pathways involving mainly dehydration, demethylation, and dehydroxylation reactions were proposed [5,59]. Firstly, OTC ($m/z = 461.1$) was transformed to A ($m/z = 479$) by hydrolysis. Then product C ($m/z = 435$) was formed from A *via* demethylation and deamination. Due to the dehydration, dehydroxylation, and decarbonylation, C was further transformed to D ($m/z = 340$). OTC was also able to be degraded to B ($m/z = 362$) through dehydration, demethylation, dihydroxylation, and deamidation. And B was transformed to D *via* dehydroxylation. In addition, the substance with B was further decomposed into the constituents with E ($m/z = 224$) and F ($m/z = 249$). Subsequently, these transformation products are oxidized to form ring opening intermediates including J ($m/z = 149$), K ($m/z = 130$), L ($m/z = 118$), and M ($m/z = 104$). Lastly, these products are mineralized into CO_2, H_2O, and additional small molecules.

This study confirmed that the metal oxide and oxygen co-doped CN prepared by one-step synthesis enhanced the catalytic efficiency and reusability of graphitic carbon nitride for contaminants degradation. In the presence of CuO/O-CN4, over 93% OTC removals were achieved, and the OTC removal rate was still as high as 91.3% after four successive runs of the synthetic catalyst. The adjustment of the electronic structure of CN by oxygen doping was conducive to the cyclic transformation of Cu(I) and Cu(II), so as to strengthen the PMS activation. The CuO/O-CN4 showed superior catalytic performance in a broad pH range of 4.3–10. Interference factors such as different kinds of anions (Cl^-, $HCO_3{}^{2-}$, $CO_3{}^{2-}$, and $NO_3{}^-$) and HA displayed a negligible impact on the removal performance of OTC in the CuO/O-CN4/PMS system. Besides, the removal efficiency of OTC in the real water environment exceeded that in the deionized water. In summary, this study provides a novel efficient PMS activator for the OTC removal in water and wastewater.

Declaration of competing interest

The authors declare no conflicts of interests.

Acknowledgments

This study was financially supported by the program for the National Natural Science Foundation of China (Nos. 52170162, 51809090, 52100182, 52100180), the Natural Science Foundation of Hunan Province, China (Nos. 2022JJ10016, 2019JJ50077, 2021JJ40087), the Science and Technology Innovation Program of Hunan Province (No. 2021RC3049), the Fundamental Research Funds for the Central Universities (No. 531118010114), the China National Postdoctoral Program for Innovative Talents (No. BX20200119), the Project Funded by China Postdoctoral Science Foundation (No. 2021M690961) and the Fundamental Research Funds for the Central Universities (No. 531118010114).

Supplementary materials

Supplementary material associated with this article can be found, in the online version, at doi:10.1016/j.cclet.2022.107893.

References

[1] P. Yang, Y. Ye, Z. Yan, et al., Chin. Chem. Lett. 32 (2021) 2823–2827.
[2] A.M. Jacobsen, B. Halling-Sørensen, F. Ingerslev, S.H. Hansen, J. Chromatogr. A 1038 (2004) 157–170.
[3] S. Lian, X. Shi, M. Lu, et al., Chem. Eng. J. 425 (2021) 130499.
[4] R. Pei, J. Cha, K.H. Carlson, A. Pruden, Environ. Sci. Technol. 41 (2007) 5108–5113.
[5] Y. Yang, C. Zhang, D. Huang, et al., Appl. Catal. B 245 (2019) 87–99.
[6] G. Chen, L.C. Nengzi, Y. Gao, et al., Chin. Chem. Lett. 31 (2020) 2730–2736.
[7] C. Zhang, S. Tian, F. Qin, et al., Water Res. 194 (2021) 116915.
[8] X.H. Jiang, F. Yu, D.S. Wu, et al., Chin. Chem. Lett. 32 (2021) 2782–2786.
[9] X. Yu, Y. Mao, D. Huang, Z. Sun, T. Li, Adv. Civ. Eng. 2021 (2021) 9934004.
[10] F. Guo, J. Lu, Q. Liu, et al., Chemosphere 205 (2018) 297–307.
[11] H. Li, C. Shan, B. Pan, Environ. Sci. Technol. 52 (2018) 2197–2205.
[12] M. Xie, J. Tang, L. Kong, et al., Chem. Eng. J. 360 (2019) 1213–1222.
[13] Q. Wang, D. Zhou, K. Lin, X. Chen, Chem. Eng. J. 419 (2021) 129667.
[14] Y. Gao, Y. Zhu, L. Lyu, et al., Environ. Sci. Technol. 52 (2018) 14371–14380.
[15] F. Chen, L.L. Liu, J.J. Chen, et al., Water Res. 191 (2021) 116799.
[16] C. He, W. Xia, C. Zhou, et al., Chem. Eng. J. 430 (2022) 132751.
[17] H. Liu, T.A. Bruton, F.M. Doyle, D.L. Sedlak, Environ. Sci. Technol. 48 (2014) 10330–10336.
[18] X. Pang, Y. Guo, Y. Zhang, B. Xu, F. Qi, Chem. Eng. J. 304 (2016) 897–907.
[19] T. Chen, Z. Zhu, Y. Bao, et al., Environ. Sci. 8 (2021) 2618–2628.
[20] J. Liu, J. Li, S. He, et al., Sep. Purif. Technol. 234 (2020) 116120.
[21] C. Zhang, Z. Ouyang, Y. Yang, et al., Chem. Eng. J. 448 (2022) 137370.
[22] S. Xu, H. Zhu, W. Cao, et al., Appl. Catal. B 234 (2018) 223–233.
[23] P.J. Larkin, M.P. Makowski, N.B. Colthup, Spectrochim. Acta, Part A 55 (1999) 1011–1020.
[24] A.C. Ferrari, S.E. Rodil, J. Robertson, Phys. Rev. B 67 (2003) 155306.
[25] L. Sun, W. Wang, C. Zhang, et al., Chem. Eng. J. 446 (2022) 137027.
[26] H. Gao, H. Yang, J. Xu, S. Zhang, J. Li, Small 14 (2018) 1801353.
[27] C. Jin, M. Wang, Z. Li, et al., Chem. Eng. J. 398 (2020) 125569.
[28] Y. Yu, S. Wu, J. Gu, et al., J. Hazard. Mater. 384 (2020) 121247.
[29] X. Yuan, S. Qu, X. Huang, et al., Chem. Eng. J. 416 (2021) 129148.
[30] Z. Wei, M. Liu, Z. Zhang, et al., Energy Environ. Sci. 11 (2018) 2581–2589.
[31] L. Lyu, D. Yan, G. Yu, W. Cao, C. Hu, Environ. Sci. Technol. 52 (2018) 4294–4304.
[32] K.A. Simonov, N.A. Vinogradov, A.S. Vinogradov, et al., ACS Nano 9 (2015) 8997–9011.
[33] C. Zhang, D. Qin, Y. Zhou, et al., Appl. Catal. B 303 (2022) 120904.
[34] H. Wang, J. Zhang, P. Wang, et al., Chin. Chem. Lett. 31 (2020) 2789–2794.
[35] L. Lyu, L. Zhang, C. Hu, Chem. Eng. J. 274 (2015) 298–306.
[36] J. Zhu, Q. He, Y. Liu, et al., J. Mater. Chem. A 7 (2019) 16999–17007.
[37] C. Song, X. Li, L. Hu, et al., ACS Appl. Mater. Interfaces 12 (2020) 8006–8015.
[38] S. Zuo, Z. Guan, D. Xia, et al., Chem. Eng. J. 420 (2021) 127619.
[39] H. Song, Z. Liu, Z. Guan, et al., Sci. Total Environ. 762 (2021) 143127.
[40] Q. Zhong, Q. Lin, R. Huang, et al., Chem. Eng. J. 380 (2020) 122608.
[41] Y.C. Lee, Y.f. Li, M.J. Chen, et al., Water Res. 174 (2020) 115618.
[42] J. Peng, H. Zhou, W. Liu, et al., Chem. Eng. J. 397 (2020) 125387.
[43] S. Wang, J. Wang, Chem. Eng. J. 385 (2020) 123933.
[44] K.Y.A. Lin, H.K. Lai, S. Tong, J. Colloid Interface Sci. 514 (2018) 272–280.
[45] R.A. Figueroa, A.A. MacKay, Environ. Sci. Technol. 39 (2005) 6664–6671.
[46] Z. Li, M. Wang, C. Jin, et al., Chem. Eng. J. 392 (2020) 123789.
[47] Y. Ji, Y. Fan, K. Liu, D. Kong, J. Lu, Water Res. 87 (2015) 1–9.
[48] R. Yuan, S.N. Ramjaun, Z. Wang, J. Liu, J. Hazard. Mater. 196 (2011) 173–179.
[49] P. Xie, J. Ma, W. Liu, et al., Water Res. 69 (2015) 223–233.

[50] W. Huang, A. Bianco, M. Brigante, G. Mailhot, J. Hazard. Mater. 347 (2018) 279–287.
[51] S.H. Ho, Y.d. Chen, R. Li, et al., Water Res. 159 (2019) 77–86.
[52] S. Guo, H. Tang, L. You, et al., Chin. Chem. Lett. 32 (2021) 2828–2832.
[53] J. Hu, H. Dong, J. Qu, Z. Qiang, Water Res. 112 (2017) 1–8.
[54] J. Ali, L. Wenli, A. Shahzad, et al., Water Res. 181 (2020) 115862.
[55] G.R. Buettner, Free Radical Biol. Med. 3 (1987) 259–303.
[56] N. Jiang, H. Xu, L. Wang, J. Jiang, T. Zhang, Environ. Sci. Technol. 54 (2020) 14057–14065.
[57] S. Wang, Y. Liu, J. Wang, Environ. Sci. Technol. 54 (2020) 10361–10369.
[58] S. Yang, P. Wu, J. Liu, et al., Chem. Eng. J. 350 (2018) 484–495.
[59] G. Fang, J. Li, C. Zhang, et al., Environ. Pollut. 300 (2022) 118939.